Integral Sliding Mode Control Based Deadbeat Predictive Current Control for PMSM Drives With Disturbance Rejection

Yongxiang Xu, *Member, IEEE*, Shaobin Li, and Jibin Zou, *Senior Member, IEEE*

***Abstract*—To promote the control performance of the modern high-precision permanent-magnet synchronous motor (PMSM) system on the existence of the time-delay and parameter mismatch, an improved deadbeat predictive current control (DPCC) method is proposed in this article. First, the conventional DPCC method considering the time-delay compensation is introduced. Along with this method, the negative influence on the control performance when the parameter mismatch occur is analyzed mathematically. Afterward, this article proposes a novel compensation scheme based on the integral sliding mode control (ISMC) theory for disturbance elimination. This proposed method incorporates the disturbance rejection term in the main control loop, which avoids the side effects of the traditional parallel external observer-based compensation method. The convergence of this disturbance rejection design is also proved. Meanwhile, the procedure of the ISMC-based DPCC method in digital implementation is illustrated and the resulting problems are discussed and solved. Furthermore, the chattering problem caused by the signum function is significantly suppressed by introducing the improved super-twisting algorithm combined method. Finally, experimental results confirm the validity of the proposed ISMC-based DPCC controller.**

***Index Terms*—Chattering attenuation, deadbeat predictive current control (DPCC), disturbance rejection, integral sliding mode control (ISMC).**

I. Introduction

A. Motivation

PERMANENT-MAGNET synchronous motors (PMSMs) are widely used in modern servo systems, such as robots and numerical-controlled machines, which require high-precision and fast tracking speed of the actuator [1]. As the inner loop of the PMSM control system, the current loop plays an important role in determining the system's performance. Hence, to achieve high-quality servo behavior, various control methods have been studied, such as hysteresis control [2], proportional–integral (PI) control [3], sliding mode control (SMC) [4], and model predictive control (MPC) [5].

Manuscript received March 7, 2021; revised July 20, 2021; accepted September 23, 2021. Date of publication September 28, 2021; date of current version November 30, 2021. Recommended for publication by Associate Editor R. Kennel. *(Corresponding author: Shaobin Li.)*

The authors are with the School of Electrical Engineering and Automation, Harbin Institute of Technology, Harbin 150001, China (e-mail: xuyx@hit.edu.cn; flyingshaobin@gmail.com; zoujibin@hit.edu.cn).

Color versions of one or more figures in this article are available at https://doi.org/10.1109/TPEL.2021.3115875.

Digital Object Identifier 10.1109/TPEL.2021.3115875

Hysteresis control boasts itself for fast response, high robustness, and simple implementation. However, the resultant unfixed switching frequency and current ripple cannot be avoided [7]. PI controllers can guarantee desired tracking precision, but the dynamic performance is not satisfactory when applied in the strongly nonlinear PMSM system [8]. SMC is a popular method to suppress external disturbance and get fast response speed, whereas the discontinuous control will cause serious chattering in the response [9]. In comparison, MPC calculates the future control signal over one or more time horizons by minimizing a predefined cost function based on the mathematical model of the plant. This method incorporates all the nonlinearities and constraints and is prone to handle multivariable systems so that it can inherit the nature of the plant and present fast dynamic response. Since the relatively heavy calculation burden compared with other control methods is solved by the improvement of microprocessors nowadays, MPC has become one of the most popular topics in power converters and drives [10].

B. Related Research

Among all the existing MPC methods, deadbeat predictive current control (DPCC) can obtain favorable performance in both dynamic and steady-state process in PMSM current control [44]. The output *dq*-axis voltages are precisely computed by the PMSM model according to the reference current. This output signal is modulated by a space vector pulsewidth modulation module before delivering to the inverter. This method is straightforward and simple and requires less calculation capacity than other MPC methods, but can ensure similar performance [5]. However, DPCCs high dependence on the motor model determines that if there exist parameter errors, unmodeled dynamics, or external disturbance, the system's behavior will be significantly damaged. In [11] and [12], the inductance mismatch will affect the dynamic state and an error larger than the real inductance value will cause instability. Unmodeled dynamics such as dead zone effect and saturation voltage drop of IGBTs will also affect the tracking precision [13]. Moreover, the one-step control period delay caused by the digital discretization is unavoidable in a real digital motor control system. This delay will cause oscillations and largely deteriorates the control performance of the overall system [14].

Plenty of papers have proposed various compensation methods to solve the problems mentioned above. As for

the aforementioned time-delay problem in a real digital control system, a simple but effective compensation method is proposed in [14]. Time-delay effect is analyzed qualitatively and a one-step ahead compensation is put forward intuitively.

The methods on tackling the parameter mismatch and unmodeled dynamics can be summarized into three main categories. The first type is to introduce a model-independent compensation term by algebraic operation using the current reference and response to cancel the steady-state error. For instance, in [15] and [16], an integral of the current tracking error is added to the *dq*-axis voltage and the convergence property is proved mathematically. A novel PI combined DPCC controller is designed with the weight decided by a fuzzy algorithm online in [6]. However, the perfect dynamic performance of the DPCC method is impaired. In [17], the tracking error of previous control period is viewed as a compensation term. Also, a carefully designed algebraic compensation term is introduced to cancel the error [22]. Even if these algebraic methods are simple but can eliminate the steady-state error, the gain is tough to tune and the robustness is hardly guaranteed when unmodeled dynamics and other disturbance exist.

Another thread is to apply the identification theory [23]. In [27], the accurate inductance value is obtained by a properly designed extraction algorithm. Also, a novel parameter identification method for the stator resistance and inductance is developed in [26] based on a reconstructed characteristic vector from the disturbance observer with current injection. Apart from identifying motor parameters, the current incremental model is constructed by a model-free linear regression form and is identified online for future voltage generation [36]. However, identification-based methods depend highly on the current measurement accuracy and largely increase calculation burden.

Meanwhile, various disturbance observer-based control methods based on separation principle manifest certain effectiveness in error suppression in DPCC [18], [19], which can be categorized into the third group. In [20] and [21], Luenberger and reduced-order Luenberger observers are applied in parallel with the main control loop to estimate the disturbance. But the requirement that the disturbance should be slowly varying is hardly met in reality. Adaptive observers also possess availability in disturbance rejection [24]. The adaptive estimation law is designed by the iterative gradient algorithm and the slowly varying assumption on the disturbance is relaxed [25]. Moreover, the extended state observer is proposed and utilized to realize the robustness in terms of flux linkage mismatch, whereas the limitation of the bandwidth and the restriction on the disturbance are the main drawbacks [27], [32]. In [28] and [30], the popular sliding mode observer based DPCC method is proposed with fast convergence speed and superior robustness, whereas the observer is updated with high-order sliding mode principle [31] and Hurwitz-based power reaching law [33] for chattering suppression and better dynamic response.

Up till now, most of the disturbance observers applied in the DPCC for parameter mismatch compensation are built in parallel with the control channel separately and the acquired estimation is then added to the controller output voltage. However, the bandwidth limitation and estimation accuracy of these external observers will restrict the current loop bandwidth more or less, not to mention that the time lag and noise in the observed disturbance will deteriorate the control performance. Hence, scholars are pursuing methods that endow the DPCCs control signal with inherent disturbance rejection ability. Recently, a novel integral sliding mode control (ISMC) theory is proposed and draws increasing attention [34], [35]. Unlike other robust control methods, ISMC incorporates the disturbance rejection term into the nominal control signal and the system's robustness is increased without sacrificing the control performance. With the advantages of the elimination of the reaching phase, which means that the disturbance is compensated from the very beginning of the operation process, ISMC has been successfully applied and proved to be effective in many applications [37]–[39].

C. Contributions

In this article, a novel ISMC based DPCC method is proposed for current control in the PMSM system with time-delay and parameter mismatch problems simultaneously solved. Also note that there is hardly any attempt to apply the ISMC theory into DPCC so far. Several practical issues for digital implementation are discussed and the proposed controller's performance is further enhanced by a super-twisting algorithm (STA) method.

The main contributions of this article are listed as follows.

1) The article creatively designs a controller for disturbance rejection of the DPCC method based on the ISMC theory. This controller can compensate the overall disturbance by the control signal itself, which has completely different structure from other disturbance observer-based compensation methods in the reference. Hence, no external observers are needed so that the control performance will not be limited by observer's performance.
2) The article solves a few practical problems caused by discretization in microprocessors of the proposed ISMC based DPCC. On the one hand, an accurate one-step ahead prediction is implemented considering the disturbance to cope with the one and a half periods' delay in the digital control system. On the other hand, a correction term is introduced to reduce the deviation of the sliding manifold caused by the nonideal tracking performance on the sudden change of the current reference.
3) Moreover, in consideration of the severe chattering phenomenon caused by the conventional signum function, an advanced STA is brought into the design to further enhance the performance of the proposed current control approach. This second-order sliding control algorithm hides the signum term inside an integral action so that the chattering in both current and speed response is significantly suppressed in essence.

The rest of this article is organized as follows. Section II introduces the conventional DPCC method with time-delay compensation for digital control systems briefly. Also, the disturbance is modeled and the tracking performance damage caused by the parameter mismatch (resistance, inductance, flux linkage) is discussed quantitatively. In Section III, the basic principle of

ISMC method is illustrated briefly. A novel DPCC combined ISMC method is proposed with its stability strictly proved. The control signal is then smoothened using a low-pass filter (LPF) and the convergence problem is further discussed. Furthermore, in Section IV, the ISMC-based DPCC with STA chattering attenuation controller is build. Experimental verification is conducted to verify the feasibility and the effectiveness of this disturbance rejection method in Section V Finally, Section VI concludes this article.

II. Conventional DPCC Method With Time-Delay Compensation

In this section, the conventional DPCC method is briefly introduced and the existing time-delay problem with its compensation method is discussed. Additionally, the overall disturbance is modeled and how the parameter mismatch affect the system's behavior is illustrated concisely.

A. Conventional DPCC and Time-Delay Compensation

In the *dq*-axis reference frame, the ideal surface mounted PMSM mathematical equation can be expressed as follows [29]:

$$\begin{bmatrix} di_d/dt \\ di_q/dt \end{bmatrix} = \begin{bmatrix} R/L & \omega_e \\ -\omega_e & R/L \end{bmatrix} \begin{bmatrix} i_d \\ i_q \end{bmatrix} + \begin{bmatrix} 1/L & 0 \\ 0 & 1/L \end{bmatrix} \begin{bmatrix} u_d \\ u_q \end{bmatrix} + \begin{bmatrix} 0 \\ -\psi_f \omega_e / L \end{bmatrix} \quad (1)$$

where u_d and u_q are the *dq*-axis voltages, i_d and i_q are the *dq*-axis currents, L is the *dq*-axis inductance, R is the stator resistance, ω_e is the electrical angular velocity, and ψ_f is the permanent-magnet flux linkage.

In an actual servo system, if the control period T is small enough, the discrete PMSM model can be acquired by the first-order Taylor series expansion as the following equation as in [28]:

$$\mathbf{i}_{dq}(k+1) = F(k)\,\mathrm{i}_{dq}(k) + G(k)\,\mathrm{u}_{dq}(k) + H(k) \quad (2)$$

where $i_{dq}(\mathrm{k}) = [\,i_d(k)\ i_q(k)\,]^{\mathrm{T}}$, $u_{\mathrm{dq}}(\mathrm{k}) = [\,\mathrm{u}_d(k)\ \mathrm{u}_q(k)\,]^{\mathrm{T}}$, $\mathbf{F}(k) = \begin{bmatrix} 1 - TR/L & T\omega_e(k) \\ -T\omega_e(k) & 1 - TR/L \end{bmatrix}$, $\mathbf{G}(k) = \begin{bmatrix} T/L & 0 \\ 0 & T/L \end{bmatrix}$, and $\mathbf{H}(k) = \begin{bmatrix} 0 \\ -T\psi_f\omega_e(k)/L \end{bmatrix}$.

The conventional DPCC method generates the voltage that allows the real current to track the reference current command exactly at the beginning of the next control period in the ideal case. This voltage signal can be computed by the discretized motor equation as follows:

$$\bar{u}_{dq}(k) = \mathbf{G}^{-1}(k)\left[\mathrm{i}^*_{dq}(k{+}1) - \mathbf{F}(k)\,\mathrm{i}_{dq}(k) - \mathbf{H}(k)\right] \quad (3)$$

where $i^*_{\mathrm{dq}}(\mathrm{k}+1) = [\,i^*_d(k+1)\ i^*_q(k+1)\,]^{\mathrm{T}}$ represents the reference current to be tracked at time $t = k{+}1$ and also means the output of the speed controller at time $t = k$.

However, due to the discrete characteristics of the digital control systems, the calculated voltage signal at time $t = k$ will be applied to the inverter at time $t = k{+}1$ and the inverter takes approximately half the current control period to exert this voltage to the motor. Therefore, this one and a half periods' delay significantly harms the system's performance [27] and will cause serious oscillation in response. To solve this issue, the most commonly adopted the one-step ahead prediction method is used. Normally, at $t = k$, the current prediction for $t = k{+}1$ is calculated according to the feedback current $i_{\mathrm{dq}}(\mathrm{k})$ as the following equation with the voltage signal $\mathrm{u}_{dq}(k)$ acquired in the previous period:

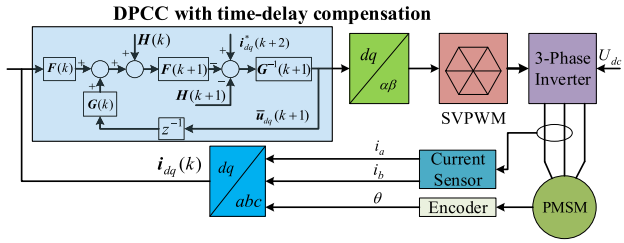

Fig. 1. Diagram of DPCC with time-delay compensation.

$$\hat{i}_{dq}(k+1) = \mathbf{F}(k)\,\mathrm{i}_{dq}(k) + \mathbf{G}(k)\,\mathrm{u}_{dq}(k) + \mathbf{H}(k). \quad (4)$$

The reference current signal $i^*_{\mathrm{dq}}(\mathrm{k}+2)$ is also needed to generate the voltage signal for $t = k{+}1$. Note that typically the speed loop control period is five to ten times larger than the current loop period (also the control period T), during which the current reference remains unchanged, so the q-axis current reference generated by the speed controller can be regarded as unchanged in the adjacent control period, that is, expression $i^*_q(\mathrm{k}{+}1) = i^*_q(\mathrm{k}+2)$ holds [8]. Since i_d is always controlled to be zero for the surface-mounted PMSM, equation $i^*_d(\mathrm{k}{+}1) = i^*_{\mathrm{d}}(\mathrm{k}+2) = 0$ fulfills. In addition, parameter matrices $\boldsymbol{F}(k)$, $\boldsymbol{G}(k)$, and $\boldsymbol{H}(k)$ can be viewed as unchanged within the adjacent current control period since the electrical angular velocity is slowly varying. Hence, the delay compensation method is deduced as the following equation and the flowchart of the whole algorithm is shown in Fig. 1:

$$\bar{u}_{dq}(k+1) = \mathbf{G}^{-1}(k)\left[\mathrm{i}^*_{dq}(k+2) - \mathbf{F}(k)\,\hat{i}_{dq}(k+1) - \mathbf{H}(k)\right] \quad (5)$$

where $\bar{u}_{dq}(k+1)$ is delivered to the inverter at time $t = k{+}1$ and the actual current $\boldsymbol{i}_{dq}(k{+}2)$ will track the current command $i^*_{\mathrm{dq}}(\mathrm{k}+2)$ at time $t = k{+}2$ ideally.

B. Disturbance Modeling and the Influence of Parameter Mismatch

If the parameter mismatch (inductance, resistance, and flux linkage) and the unmodeled dynamics are considered in the PMSM model, (1) can be reconstructed as the following equation:

$$\begin{cases} \frac{di_d}{dt} = \frac{1}{L_0}u_d - \frac{R_0}{L_0}i_d + \omega_e i_q + f_d \\ \frac{di_q}{dt} = \frac{1}{L_0}u_q - \frac{R_0}{L_0}i_q - \omega_e i_d - \frac{\psi_f \omega_e}{L_0} + f_q \\ f_d = (\frac{1}{L} - \frac{1}{L_0})u_d - (\frac{R}{L} - \frac{R_0}{L_0})i_d + \varepsilon_d \\ f_q = (\frac{1}{L} - \frac{1}{L_0})u_q - (\frac{R}{L} - \frac{R_0}{L_0})i_q - (\frac{\psi_f}{L} - \frac{\psi_{f0}}{L_0})\omega_e + \varepsilon_q. \end{cases} \quad (6)$$

Parameters with subscript "0" denote the nominal value used in the DPCC controller for voltage generation. Additionally, f_d and f_q are lumped disturbance, which comprise the unmodeled dynamics ε_d and ε_q and the error caused by parameter incongruity. Clearly, the disturbance term is responsible for the imperfect tracking performance. If the unmodeled dynamics terms are neglected, the influence of parameter mismatch in the transient and steady state can be evaluated theoretically. By combining (2) and (5), the following equations can be derived to represent how the parameter mismatch affects the q-axis current tracking performance (d-axis current has similar tracking performance) in terms of inductance, resistance, and flux linkage, respectively:

$$\begin{aligned} &i_q(k+1) - {i^*}_q(k+1) \\ &= -\frac{\Delta L}{L}[{i^*}_q(k+1) - i_q(k-1) - 2T\omega_e(k-1)i_d(k-1)] \end{aligned} \tag{7}$$

$$i_q(k+1) - {i^*}_q(k+1) = -\frac{2T\Delta R}{L} i_q(k-1) \tag{8}$$

$$i_q\,(k+1) - i_q^*\,(k+1) = -\frac{2T\Delta\psi_f}{L}\omega_e(k-1) \tag{9}$$

where $\Delta L = L - L_0$, $\Delta R = R - R_0$, and $\Delta\psi_f = \psi_f - \psi_{f0}$.

As for the steady-state error, (7)–(9) show that the q-axis current tracking error is proportional to the difference between the parameter's real value and nominal value. Meanwhile, if the parameter error is fixed, the tracking error also grows proportionally with the reference current value when only inductance and resistance mismatches occur. Under the flux linkage mismatch, the tracking error is related to the electrical angular velocity, which means that with higher ω_e, the tracking error grows larger.

As for the transient process, conclusions can be drawn through transfer function analysis and discrete time system theory [40]. The inductance error affects the dynamic process with the setting time prolonged and if the nominal value is bigger than the real value, oscillation in response occurs. The negative influence dynamically caused by the flux linkage and resistance error is tiny compared with the inductance mismatch but still not negligible [11].

Therefore, to maintain good tracking performance with the presence of disturbance both in transient and steady states, it is necessary to compensate these undesired terms.

III. Proposed ISMC-Based DPCC Method and Digital Implementation Procedure

Based on previous analysis, even if the time-delay compensation strategy is adopted in the DPCC method, the lumped disturbance will degrade the control performance largely. In other words, the unavoidable steady-state error will affect the system's tracking accuracy and prolong the tracking speed. In this section, a novel disturbance rejection method is put forward with the compensation signal embedded in control which both solve time-delay issue and help the system insensitive to parameter mismatch and unmodeled dynamics. First, the basic principle of ISMC method is briefly introduced. Then, the composite control structure of the ISMC-based DPCC is illustrated and the convergence of this combined method is strictly proofed. Afterward, a correction term is introduced for sliding surface optimization and finally digital implementation procedure of this proposed method is summarized.

A. Principle of the ISMC Method

The ISMC is a powerful control method that eliminates the reaching phase by enforcing the sliding mode to happen throughout the entire process. On account of this property, system's robustness will be guaranteed from the initial time instant. Recently, this method has drawn much attention since Utkin *et al.* first proposed it in [41] and it has revealed effectiveness in many practical applications.

Consider a system represented by a state equation in the following equation that contains certain unknown disturbance:

$$\dot{x} = f(x) + B(x)u + h(x) \tag{10}$$

where $x \in \Re^n$ is the state vector, $u \in \Re^m$ is the input vector, $B(x) \in \Re^{n\times m}$, $f(x) \in \Re^n$, and the disturbance vector $h(x) \in \Re^n$ is bounded by positive values h_i^+ with $|h_i| \le h_i^+$, $i = 1, 2, \ldots, n$.

The control purpose of the ISMC is to find a control u consisting of two parts, i.e., $u = u_0 + u_1$, where an auxiliary control signal u_1 is used for disturbance rejection and the main control u_0 navigates the states to follow the desired trajectory. According to [34], an integral sliding manifold is typically designed as follows:

$$s(x) = s_0(x) + z. \tag{11}$$

The first part in (11), which is $s_0(x)$, is usually constructed as a linear combination of the system states. Also, to acquire the disturbance rejection ability, $\dot{z}$ is chosen as follows to cancel out the known part of the system such that only control u_1 and disturbance term $h(x)$ exists in the time derivative of the sliding variable s:

$$\begin{cases} \frac{dz}{dt} = -\frac{\partial s_0}{\partial x}(f(x) + B(x)u_0) \\ z(0) = -\,s_0(x(0)). \end{cases} \tag{12}$$

Additionally, an initial condition is necessary to ensure $s(x) = 0$ holds at the starting time, which is calculated as the second expression in (12). Furthermore, if a properly designed auxiliary control signal u_1, such as signum function, ensures the convergence of the sliding variable s to 0, then the disturbance can be rejected and estimated completely.

From (10)–(12), if $s(x) = 0$ holds, the disturbance information is contained in the equivalent control of u_1, which is denoted as $u_{1\mathrm{eq}}$ in the following equation, and the disturbance $h(x)$ can thus be fully compensated by u_1:

$$-B(x)u_{1\mathrm{eq}} = h(x). \tag{13}$$

B. ISMC-Based DPCC Controller Design

Consider the PMSM equation with disturbance in (6). The DPCC method is chosen as the main control u_0 for the high-quality tracking performance and another term u_1 is designed based on the procedure of ISMC previously discussed for disturbance rejection. The sliding manifold consists of merely the

current tracking error and the auxiliary variable z since the system's relative degree is one, which is written as follows:

$$\mathbf{s}_{dq} = \begin{bmatrix} s_d \\ s_q \end{bmatrix} = \begin{bmatrix} i_d - i_d^* + z_d \\ i_q - i_q^* + z_q \end{bmatrix}. \tag{14}$$

According to (12), $\boldsymbol{z}_{dq}$ can be designed as follows along with the initial values:

$$\begin{aligned} \tfrac{d\mathbf{z}_{dq}}{dt} &= \begin{bmatrix} dz_d/dt \\ dz_q/dt \end{bmatrix} \\ &= \begin{bmatrix} -(u_{d0}/L_0 - R_0 i_d/L_0 + \omega_e i_q) + di_d^*/dt \\ -(u_{q0}/L_0 - R_0 i_q/L_0 - \omega_e i_d - \psi_f \omega_e/L_0) + di_q^*/dt \end{bmatrix} \\ \mathrm{z}_{dq}(0) &= \begin{bmatrix} -(i_d(0) - i_d^*(0)) \\ -(i_q(0) - i_q^*(0)) \end{bmatrix}. \end{aligned} \tag{15}$$

Consequently, after combining (14) and (15), the time derivative of the sliding manifold takes the simple form of the following equation:

$$\dot{\mathbf{s}}_{dq} = \begin{bmatrix} \dot{s}_d \\ \dot{s}_q \end{bmatrix} = \begin{bmatrix} u_{d1}/L_0 + f_d \\ u_{q1}/L_0 + f_q \end{bmatrix}. \tag{16}$$

Note that u_{d0} and u_{q0} denote the *dq*-axis voltages generated by the DPCC controller, whereas u_{d1} and u_{q1} are designed based on the ISMC algorithm. If the sliding motion happens, which means that (16) is equal to zero, the *dq*-axis disturbance can be accurately estimated by the auxiliary control signal.

Proposition 1: Consider the PMSM system (6) and an integral sliding manifold designed by (14) and (15), s_d and s_q can stay identically to the origin from the initial time instant if the disturbance rejection control $\boldsymbol{u}_{dq1}$ is chosen as follows:

$$\mathbf{u}_{dq1} = \begin{bmatrix} u_{d1} \\ u_{q1} \end{bmatrix} = \begin{bmatrix} -M_d \mathrm{sgn}(\mathrm{s}_d) \\ -M_q \mathrm{sgn}(\mathrm{s}_q) \end{bmatrix} \tag{17}$$

where M_d and M_q are the constants satisfying $M_d > \max\{|L_0 f_d|\}$ and$M_q > \max\{|L_0 f_q|\}$, and symbol "sgn" denotes signum function.

Proof: Since the motor equations in the *dq*-axis take the same forms, s_d is taken for analysis. Consider a Lyapunov candidate as follows:

$$V_d = s_d^2/2 \tag{18}$$

which is a positive definite function except at the origin and is globally continuously differentiable. The purpose is to find a proper range for constant M_d so that V_d can converge to the origin.

According to the Lyapunov stability theorem, the time derivative of V_d can be expressed and simplified as follows:

$$\begin{aligned} \dot{V}_d &= \dot{s}_d s_d = s_d(u_{d1}/L_0 + f_d) \\ &= s_d(f_d - M_d \mathrm{sgn}(\mathrm{s}_d)/L_0) \\ &\le |s_d|\,(|f_d| - M_d/L_0). \end{aligned} \tag{19}$$

To ensure that $\dot{V}_d$ is negative, parameter M_d in disturbance rejection control (17) should satisfy as follows:

$$M_d > \max\{|L_0 f_d|\}. \tag{20}$$

Obviously, if the condition in (20) is fulfilled, the inequality (19) is smaller than 0 globally except at the origin $s_d = 0$. When the condition V_d reaches infinity when s_d tends to infinity holds, the origin is a globally asymptotically stable point. Also, when the initial condition in (15) is chosen, $s_d(0) = 0$ holds at the initial time $t = 0$. Afterward, the nonpositive Lyapunov function forces the sliding manifold s_d to stay at the origin throughout the whole process, which means that equation $s_d = \dot{s}_d = 0$ holds. Hence, the disturbances f_d and f_q can be expressed by the equivalent control as follows:

$$\begin{cases} f_d = -u_{d1\mathrm{eq}}/L_0 \\ f_q = -u_{q1\mathrm{eq}}/L_0. \end{cases} \tag{21}$$

From the analysis above, the ISMC-based DPCC method can be denoted by the combined control signal $\mathbf{u}_{dq} = \mathbf{u}_{dq0} + \mathbf{u}_{dq1}$, where $\boldsymbol{u}_{dq1}$ is responsible for disturbance rejection and $\boldsymbol{u}_{dq0}$ inherits the merits of the conventional DPCC. However, the signum-type discontinuous term $\boldsymbol{u}_{dq1}$ will cause sudden change in the PWM duty cycle, which is harmful to the inverter and will also bring in chattering in the response [42]. Typically, an LPF is added before the control signal is delivered to the inverse Park transformation for smoothness whose transfer function is written as follows in the complex frequency domain (with high-frequency components filtered out, the equivalent value of the discontinuous control can be used for disturbance elimination, which is denoted as $\boldsymbol{u}_{dq1\mathrm{eq}}$):

$$\frac{\mathbf{u}_{dq1\mathrm{eq}}}{\mathbf{u}_{dq1}} = \frac{1}{(\tau_{dq} s + 1)} \tag{22}$$

where $u_{\mathrm{dq1eq}} = [\,\mathrm{u}_{d1\mathrm{eq}}(k)\ \mathrm{u}_{\mathrm{q1eq}}(k)\,]^{\mathrm{T}}$, and τ_{dq} denotes the LPF gain matrix containing tunable coefficients τ_d and τ_q.

By applying this LPF to the control signal, the convergence condition in Proposition 1 becomes stricter, which means that constants M_d and M_q should satisfy the following equation to ensure the convergence of the designed integral sliding manifold in (14):

$$\begin{cases} M_d > \max\{|L_0 f_d + u_{d1\mathrm{eq}} - u_{d1}|\} \\ M_q > \max\{|L_0 f_q + u_{q1\mathrm{eq}} - u_{q1}|\}. \end{cases} \tag{23}$$

Compared with the conventional DPCC method, four more parameters (M_d, M_q, τ_d, and τ_q) are introduced in this disturbance rejection control signal $\boldsymbol{u}_{dq1}$. The tuning of M_d and M_q is a tradeoff between the robustness to the lumped disturbance f_d and f_q and the undesired chattering phenomenon in the current response. A higher M_d and M_q value endows stronger antidisturbance ability to the system because higher f_d and f_q are tolerable for the convergence of the sliding manifold. That is, if the parameters deviate from real values to a considerable extent, the gains M_d and M_q need to be adjusted larger and vice versa. Meanwhile, the maximum available values can be obtained by trial and error for an acceptable chattering level in the response. As for the coefficients τ_d and τ_q in an LPF, a larger value means a lower filter cutoff frequency and a smaller chattering level while the difference between u_{dq1eq} and u_{dq1} grows bigger. Hence, the enlarged value on the right-hand side of (23) will reduce the antidisturbance property of the ISMC control signal in return, which is the cost of filtering. In conclusion, large enough M_d and M_q should be ensured while τ_d and τ_q can be further tuned for a desirable chattering level.

C. Correction Term and Sliding Surface Optimization

In reality, the change rate of *dq*-axis currents has an upper bound because of the electric time constant of the motor. As a result, the actual current response is not able to follow the sudden change of the reference signal, for example, a step, in the first few control periods. Take the *d*-axis current tracking performance for clear illustration. If the time-delay issue is not considered, from (2), (3), (14), and (15), the time derivative of the *d*-axis component of the sliding variable s_d can be described as follows after discretization:

$$s_d(k+1) = [i_d(k+1) - i_d^*(k+1)] + s_d(k). \tag{24}$$

Clearly in this case, the time derivative of s_d cannot stay identically to zero before the reference *d*-axis current is tracked. In this dynamic process, $s_d(k+1)$ cumulates monotonously departing zero under this integral-like action before it is pulled back to the origin by the ISMC control action after the real *d*-axis current completely tracks the reference. The ISMC algorithm will not take effect during this period.

To solve this problem, the error between the reference current and the predicted value at $t = k{+}1$ is multiplied by a tunable weighing factor η_{dq}, which is selected within the range of (0, 1) as (25), and this term $\boldsymbol{z}_{dqc}(k{+}1)$ is then added to the discretized auxiliary variable $\boldsymbol{z}_{dq}(k{+}1)$ in (28) for sliding variable correction. By this tunable correction term, the undesired difference between the feedback and reference currents in the right-hand side of (24) can be canceled partially when the sudden change of current command happens and the dynamic performance of this ISMC-based DPCC method will get largely enhanced

$$\mathbf{z}_{dqc}(k+1) = \begin{bmatrix} \eta_d(i_d^*(k+1) - \hat{i}_d(k+1)) \\ \eta_q(i_q^*(k+1) - \hat{i}_q(k+1)) \end{bmatrix} \tag{25}$$

where $\eta_{dq} = [\eta_d \ \eta_q]^T$.

The selection of η_{dq} determines the ability that the sliding manifold s_d and s_q hold at the origin on the sudden change of the current reference. A properly designed weighing factor η_{dq} can assure acceptable deviation from the origin and a shorter recovery time for the sliding manifold to converge to zero during the transient process. However, an overdesigning of the weighing factor will cause overshoot of the sliding manifold. Therefore, η_{dq} should be carefully tuned by trial and error in practical applications for the best performance.

D. Digital Implementation of the Proposed Method

The implementation procedure of the proposed ISMC-based DPCC method can be summarized into five steps considering the disturbance rejection and time-delay compensation as in Fig. 2. Assume that at time $t = k$, the acquired states are the feedback current $\boldsymbol{i}_{dq}(k)$, the electrical angular velocity $\omega_e(k)$, and the reference current $i_{dq}^*(\mathrm{k}+1)$ from the speed controller.

1) One-Step Ahead Current Prediction: The current prediction formula is written as follows from which the predictive current of the next sampling point $\hat{i}_{dq}(k+1)$ is computed (note that the disturbance term should be considered for the accurate

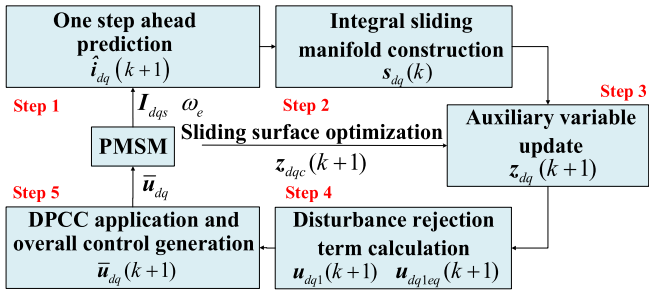

Fig. 2. Digital implementation procedure of the proposed ISMC based DPCC.

prediction):

$$\hat{i}_{dq}(k+1) = \mathbf{F}(k)\,\mathrm{i}_{dq}(k) + \mathbf{G}(k)\,\mathrm{u}_{dq}(k) + \mathbf{H}(k) + \mathrm{F}_{dq}(k) \tag{26}$$

where $F_{\mathrm{dq}}(\mathrm{k}) = [\,\mathrm{f}_d(k)\ \mathrm{f}_q(k)\,]^{\mathrm{T}}$ represents the disturbance matrix.

2) Integral Sliding Manifold Construction: The sliding manifold in (14) can be discretized as follows in microprocessors:

$$\mathbf{s}_{dq}(k) = \begin{bmatrix} s_d(k) \\ s_q(k) \end{bmatrix} = \begin{bmatrix} i_d(k) - i_d^*(k) + z_d(k) \\ i_q(k) - i_q^*(k) + z_q(k) \end{bmatrix}. \tag{27}$$

3) Auxiliary Variable z *Update:* From (15), forward Euler discretization with the step size T is applied to deal with the time derivative in the continuous time domain and the resultant $\boldsymbol{z}_{dq}(k{+}1)$ is updated by the following equation for the execution in the next control period with $\boldsymbol{z}_{dqc}(k{+}1)$ included:

$$\begin{aligned} \mathrm{z}_{dq}(k+1 = \mathbf{z}_{dq}(k) + \mathbf{i}_{dq}^*(k+1) - \mathbf{i}_{dq}^*(k) \\ - ((\mathbf{F}_0 - \mathbf{I})\mathbf{i}_{dq}(k) + \mathbf{G}_0\mathrm{u}_{dq0}(k) + \mathbf{H}_0) + \mathrm{z}_{dqc}(k+1). \end{aligned} \tag{28}$$

4) Disturbance Rejection Term Calculation: In this step, the disturbance rejection part of the control signal $\boldsymbol{u}_{dq1}(k{+}1)$ is calculated as the following equation from (17)

$$\mathbf{u}_{dq1}(k+1) = -\mathbf{M}_{dq}\mathrm{sgn}(\mathbf{s}_{dq}(k)) \tag{29}$$

and is transferred to a post LPF filter as the following equation for smoothness, where $\boldsymbol{u}_{dq1\mathrm{eq}}(k{+}1)$ denotes the output of the LPF filter (note that $\boldsymbol{M}_{dq}$ must satisfy the condition in (23), whereas the LPF gain τ_{dq} is tunable to get the best performance):

$$\mathbf{u}_{dq1\mathrm{eq}}(k+1) = T \cdot \mathbf{u}_{dq1}(k)/\tau_{dq} + (1 - T/\tau_{dq}) \cdot \mathbf{u}_{dq1\mathrm{eq}}(k) \tag{30}$$

where $\mathrm{M}_{dq} = [\,M_d\ M_q\,]^T$.

5) DPCC Application and the Overall Control Generation: Here the DPCC method adopts the aforementioned delay compensation algorithm in expression (5) in Section II to remove the time-delay influence. Also, the overall control signal containing DPCC and ISMC disturbance suppression is written as follows, which is also the signal addressed to the inverse Park transformation:

$$\bar{\mathbf{u}}_{dq}(k+1) = \mathbf{u}_{dq1\mathrm{eq}}(k+1) + \bar{\mathbf{u}}_{dq0}(k+1) \tag{31}$$

where $\bar{u}_{\mathrm{dq0}}(\mathrm{k}+1) = [\,\bar{u}_{\mathrm{d0}}(\mathrm{k}+1)\ \bar{u}_{q0}(\mathrm{k}+1)\,]^{\mathrm{T}}$ is the calculated DPCC control voltage value from (5).

In conclusion, the five steps above clearly illustrate the digital implementation procedure of the proposed ISMC based DPCC

in a real microprocessor. When one cycle is finished, the program returns to Step 1) and a new circulation begins.

IV. Improved ISMC-Based DPCC With STA Chattering Attenuation Scheme

In the previous analysis, although disturbance is effectively compensated by the proposed ISMC based DPCC method, the side effect that severe chattering will be brought in the tracking response by the conventional signum function is not negligible. To suppress this impact and further improve the disturbance rejection behavior, a superior second-order sliding mode STA method is incorporated into the conventional ISMC for a better performance, which is the main contribution of this section.

The STA method belongs to the second-order sliding mode category but is suitable for dealing with relative degree one systems [42]. It can force the sliding manifold itself and its first-order time derivative converges to the origin in finite time without the necessity of acquiring the time derivative of the sliding variable. Another advantage is that the second-order sliding nature conceals the discontinuous control term inside an integral operation, thus eliminating the undesired chattering phenomenon.

The standard STA method can be formulated as (32) where s is a predefined sliding surface [34]. Its strict proof can be found in [43] by Lyapunov stability criterion and the sliding variable s possesses a finite-time convergence feature

$$\begin{aligned} \dot{s} &= -k_1\sqrt{|s|}\mathrm{sgn}(s)+\mathrm{v} \\ \dot{v} &= -k_2\mathrm{sgn}(s)+\rho, |\rho|<L \end{aligned} \tag{32}$$

where ρ represents the unknown term or disturbance with a constant upper boundary L and the gains are usually chosen as $k_1=1.5\sqrt{L}$ and $k_2=1.1L$ for a good compromise between fast convergence and high accuracy [35].

To further improve the control performance of the proposed ISMC-based DPCC method, the conventional signum function, which is discontinuous, is replaced by the STA convergence law above. Based on (16), assume that the time derivative of the disturbance terms are bounded by constants h_d and h_q, which means that condition $|\dot{f}_d|<h_d$ and $|\dot{f}_q|<h_q$ fulfills. Clearly, it is a relaxation of the disturbance constraint compared with other observer-based methods and the restriction condition in the STA method satisfies a more general case. Meanwhile, the auxiliary control signals u_{d1} and u_{q1} are designed as (33) so that the sliding mode behavior is in the same form as the formula in (32), whose convergence is guaranteed. Hence, the integral sliding variable $\boldsymbol{s}_{dq}$ will converge to zero in finite time and the disturbance estimation (21) holds

$$\begin{aligned} \mathbf{u}_{dq1} &= L_0\left(-\mathbf{k}_{dq1}\sqrt{|\mathbf{s}_{dq}|}\mathrm{sgn}(\mathbf{s}_{dq})+\mathbf{v}_{dq}\right) \\ \dot{\mathbf{v}}_{dq} &= -\mathbf{k}_{dq2}\mathrm{sgn}(\mathbf{s}_{dq}) \end{aligned} \tag{33}$$

where $k_{\mathrm{dq1}}=[\mathrm{k}_{d1}\ \mathrm{k}_{q1}]^{\mathrm{T}}$ and $k_{\mathrm{dq2}}=[\mathrm{k}_{d2}\ \mathrm{k}_{q2}]^{\mathrm{T}}$ are the gain matrices fulfilling $\mathbf{k}_{dq1}=1.5\sqrt{\mathbf{h}_{dq}}$, $\mathbf{k}_{dq2}=1.1\mathbf{h}_{dq}$, and $h_{\mathrm{dq}}=[\mathrm{h}_d\ \mathrm{h}_q]^{\mathrm{T}}$.

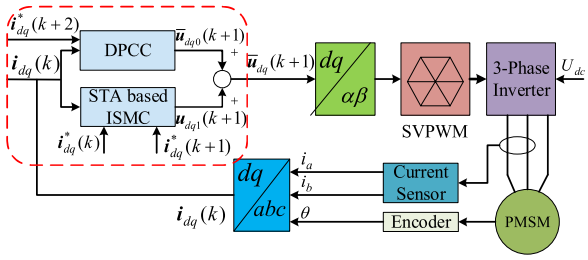

Fig. 3. Diagram of the proposed ISMC-based DPCC with chattering attenuation.

TABLE I
Parameters Related to the Test Motor

Parameters	Value	Unit
DC link voltage	120	V
Rated speed	1000	rpm
Pole pairs	5	
Phase resistance	0.7166	Ω
dq-aixs inductance	1.2	mH
Flux linkage	0.059333	Wb

Fig. 3 depicts the diagram of the proposed ISMC-based DPCC with STA chattering attenuation. The dq-axis current feedback and current references are delivered to the STA based ISMC block and then the desired disturbance rejection control signal $\mathbf{u}_{dq1}(k+1)$ is calculated. Furthermore, the digital implementation of the proposed ISMC-based DPCC with STA method is similar to the one illustrated in Section III except that Step 4) is replaced by this new control signal in (34). Since (34) is a continuous control signal, the chattering phenomenon can be significantly attenuated, whereas the same disturbance rejection ability can be realized.

Also note that the selection of coefficients h_d and h_q is similar to the rules for M_d and M_q in Section III. From the analysis above, h_d and h_q are the upper bounds of the time derivative of disturbance and the larger these values are, the stronger disturbance ability is endowed to the system. Since chattering is significantly attenuated by this proposed STO and ISMC combined method, h_d and h_q can be tuned relatively higher for a better antidisturbance property.

$$\begin{aligned} \mathbf{u}_{dq1}(k+1) = L_0\cdot\left(-\mathbf{k}_{dq1}\sqrt{|\mathbf{s}_{dq}(k)|}\mathrm{sign}(\mathbf{s}_{dq}(k))\right) \\ +T\cdot\sum_{n=0}^{k}\left(-\mathbf{k}_{dq2}\mathrm{sign}(\mathbf{s}_{dq}(\mathrm{k}))\right). \end{aligned} \tag{34}$$

V. Experimental Results

To verify the effectiveness of this proposed ISMC combined DPCC method, experiments are performed on a PMSM digital control system platform in Fig. 4. The PMSM used in the experiment is a surface-mounted type with the electrical and mechanical parameters listed in Table I. The experimental setup is built based on the TMS320F28335 microprocessor. The PWM frequency is set as 10 kHz and the corresponding current loop

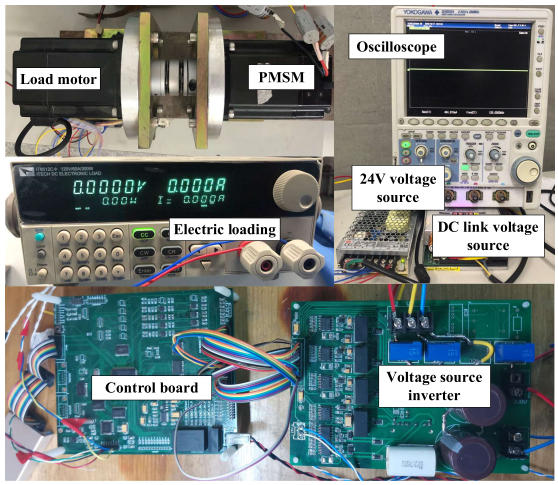

Fig. 4. Actual PMSM experimental platform.

and speed loop control frequencies are as 10 kHz and 2 kHz, respectively. Also, the dead zone time is set as 1 μs.

The experimental results of the three controllers on d-axis current tracking performance are given in Figs. 5 and 6. The amplitude of the step excitation is 4 A. Under this excitation, the first experiment is done when no parameter mismatch is added and the results are displayed in Fig. 5. Fig. 5(a) shows the d-axis reference i^*_d and the performance of the corresponding response i_d. Clearly, the rise time is about 1.2 ms, which means that transient state is good enough. However, the measured i_d feedback only reaches 3.83 A with a 0.17-A tracking error because of the nonideal inverter and the dead zone effect, which handicaps the high-quality tracking performance. When the ISMC-based DPCC with signum function is applied in Fig. 5(b), good transient performance retains (1.1 ms), whereas the steady-state error is equivalently offset with the parameter properly tuned. Also, in this figure, the disturbance $f_{\rm d}$ is roughly estimated. However, even if the steady error is compensated, the current response clearly appears an obvious chattering phenomenon. In comparison, the chattering is significantly reduced in terms of amplitude when the conventional signum function is replaced by the STA algorithm in Fig. 5(c). Meanwhile, it can be seen that satisfying tracking performance still remains (1.1 ms) when the improved ISMC-based DPCC method is applied. The corresponding sliding surface s_d and the estimated disturbance f_d are exhibited and the convergence phase of s_d in the sudden change of current command proves the analysis in Section III, which means that the correction term is a necessity.

In Fig. 6(a), if the parameter mismatches are taken into account ($R_0 = 0.5R$, $L_0 = 0.5L$, and $\psi_{f0} = 0.5\psi_f$), the tracking error of conventional DPCC in the steady state enlarges to about 0.814 A, whereas the rise time prolongs a little to 2.2 ms. This tracking error is not acceptable in the high-quality tracking applications. With the ISMC signal applied in Fig. 6(b) and (c), the equivalent recursive mean square (RMS) value of the response is 4 A with the tracking error completely canceled. In Fig. 6(b), the rise time (6 ms) becomes longer than that without compensation. The chattering is not negligible in this case, whose amplitude

TABLE II
TRACKING ERROR UNDER PARAMETER MISMATCHES ON CONSTANT LOAD TORQUE OF 1 N·M

Value	Parameter difference	DPCC		DPCC+ISMC		DPCC+ISMC+STA	
		Δi_d/A	Δi_q/A	Δi_d/A	Δi_q/A	Δi_d/A	Δi_q/A
$\Delta\psi_f$	$0.5\psi_f$	-0.41	1.38	0.005	0.027	0.002	0.047
	0	-0.42	0.26				
	$-0.5\psi_f$	-0.42	-0.87				
ΔR	$0.9R$	-0.46	0.21	0.009	0.05	0.02	0.035
	0	-0.46	0.05				
	$-R$	-0.54	0.15				
ΔL	$0.5L$	-0.87	0.52	0.017	0.039	0.022	0.031
	0	-0.41	0.15				
	$-0.5L$	-0.20	0.10				

reaches 0.28 A. If the STA method is combined, it is obvious that the rise time 1.8 ms is smaller than in Fig. 6(a) and the chattering is prominently eliminated compared with Fig. 6(b) in the current response, sliding surface s_d, and the disturbance estimation f_d, which is fairly acceptable. Additionally, in the situation with not negligible parameter errors, the related gains (k_d, k_q, M_d, and M_q) should be tuned larger than those in the case in Fig. 5.

Figs. 6–9 display the dq-axis currents' performance when the motor operates at rated speed 1000 r/min and constant load 1 N·m. In Fig. 7, the nominal flux linkage value ψ_{f0} in the algorithm changes from $0.5\psi_f$ to ψ_f suddenly, and then increases to $1.5\psi_f$ with the other two parameters (inductance and resistance) unchanged. The duration for each value is 1.2 s. Figs. 8 and 9 follow the same operating condition, whereas the variable parameters become the motor resistance and inductance, respectively. All figures denoted by (a) in Figs. 7–9 demonstrate the behavior under the conventional DPCC method. From the above analysis, the current errors are comprised of the nonideal inverter effect and the parameter mismatch part and are particularly not negligible in the steady state. Through study, the flux linkage difference deteriorates the q-axis current tracking performance most in terms of transient state and steady state, whereas inductance difference affects the d-axis current tracking performance most. The maximum tracking error of dq-axis currents are about 1.38 A and 0.87 A, respectively. Meanwhile, all (b) in Figs. 7–9 show the effectiveness of the proposed ISMC-based DPCC method with signum function and all (c) depict the condition applying STA algorithm. Table II illustrates the RMS value difference between the dq-axis current reference and response in this constant load torque case. It can be seen that the tracking error in the steady state is fully compensated (below 0.05 A) by the proposed algorithm although tiny fluctuation occurs on the moment of the nominal motor values' sudden change with the gains (M_d, M_q, τ_d, τ_q, η_d, and η_d) properly chosen. Additionally, better performance can be observed if the STA algorithm is implemented with the fluctuation amplitude and duration reduced. Note that when the motor works under the rated speed and load, the chattering phenomenon is almost invisible compared with the conventional DPCC both in signum function and the STA method.

To further verify the q-axis tracking ability and the disturbance rejection property of the proposed algorithm with parameter

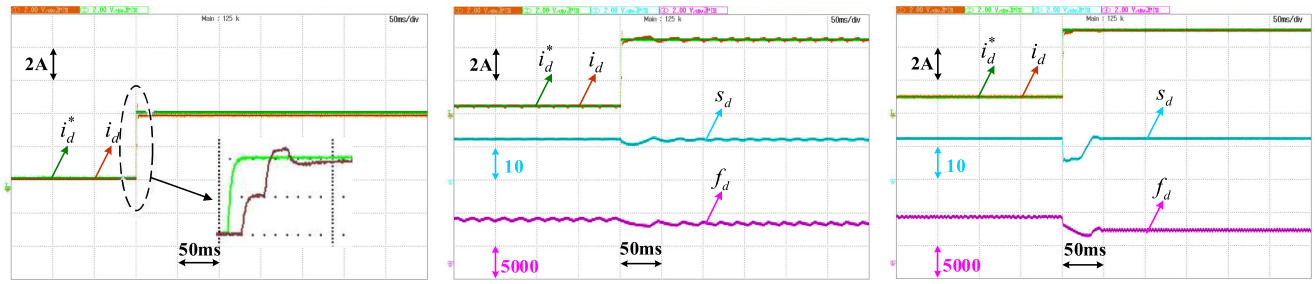

(a) (b) (c)

Fig. 5. Comparison of three controllers at the step change of i_d in the amplitude from 0 to 4 A without parameter mismatch. (a) Conventional DPCC. (b) ISMC-based DPCC ($M_d = 2$, $\tau_d = 200$, and $\eta_d = 0.7$). (c) ISMC-based DPCC with STA chattering attenuation ($h_d = 10\,000$ and $\eta_d = 0.6$).

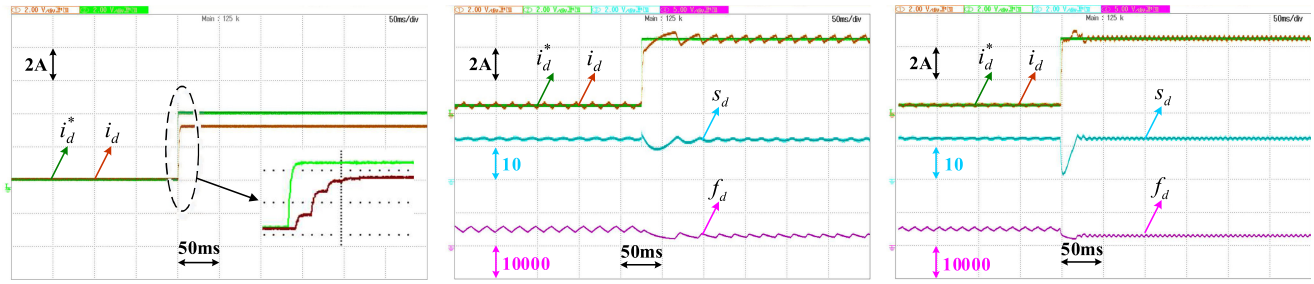

(a) (b) (c)

Fig. 6. Comparison of three controllers at the step change of i_d in the amplitude from 0 to 4 A with $R_0 = 0.5R$, $L_0 = 0.5L$, and $\psi_{f0} = 0.5\psi_f$. (a) Conventional DPCC. (b) ISMC-based DPCC ($M_d = 4$, $\tau_d = 200$, and $\eta_d = 0.94$). (c) ISMC-based DPCC with STA chattering attenuation ($h_d = 200\,000$ and $\eta_d = 0.36$).

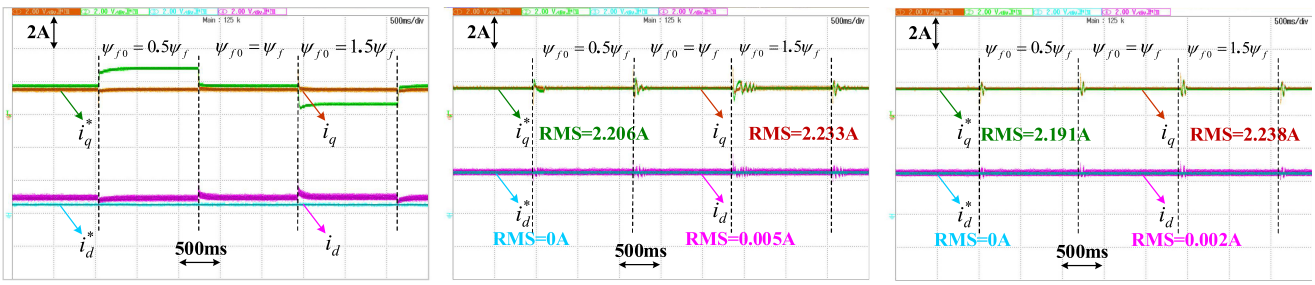

(a) (b) (c)

Fig. 7. Comparison of three controllers in current performance in the steady state when flux mismatch occurs under 1000 r/min and 1 N·m. (a) Conventional DPCC. (b) ISMC-based DPCC ($M_d = 10$, $M_q = 20$, $\tau_d = \tau_q = 200$, $\eta_d = 0.8$, and $\eta_d = 0.99$). (c) ISMC-based DPCC with STA chattering attenuation ($h_d = 50\,000$, $\eta_d = 0.6$, $h_q = 500\,000$, and $\eta_d = 0.64$).

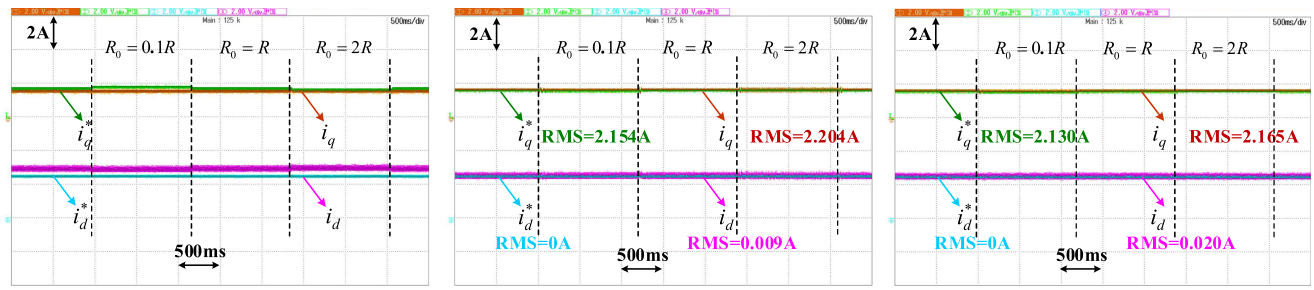

(a) (b) (c)

Fig. 8. Comparison of three controllers in current performance in the steady state when resistance mismatch occurs under 1000 r/min and 1 N·m. (a) Conventional DPCC. (b) ISMC-based DPCC ($M_d = 7$, $M_q = 6$, $\tau_d = \tau_q = 200$, $\eta_d = 0.92$, and $\eta_d = 0.99$). (c) ISMC-based DPCC with STA chattering attenuation ($h_d = 50\,000$, $\eta_d = 0.6$, $h_q = 300\,000$, and $\eta_d = 0.8$).

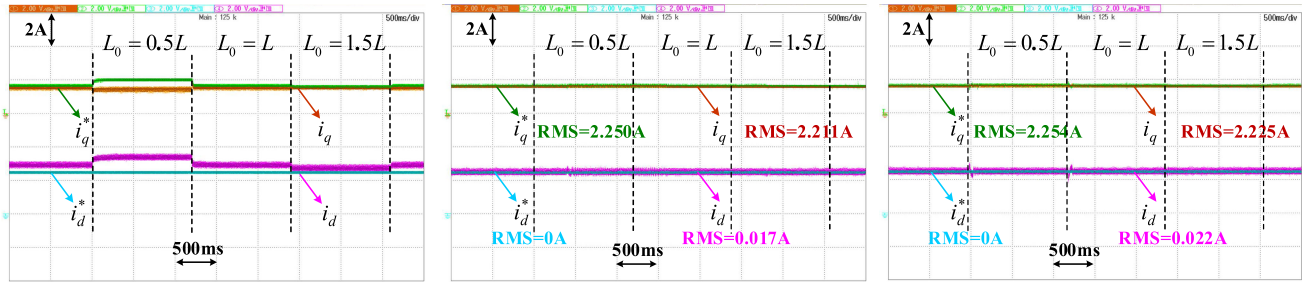

Fig. 9. Comparison of three controllers in current performance in the steady state when inductance mismatch occurs under 1000 r/min and 1 N·m. (a) Conventional DPCC. (b) ISMC-based DPCC ($M_d = 8$, $M_q = 6.4$, $\tau_d = \tau_q = 200$, $\eta_d = 0.92$, and $\eta_d = 0.99$). (c) ISMC-based DPCC with STA chattering attenuation ($h_d = 150\,000$, $\eta_d = 0.5$, $h_q = 300\,000$, and $\eta_d = 0.9$).

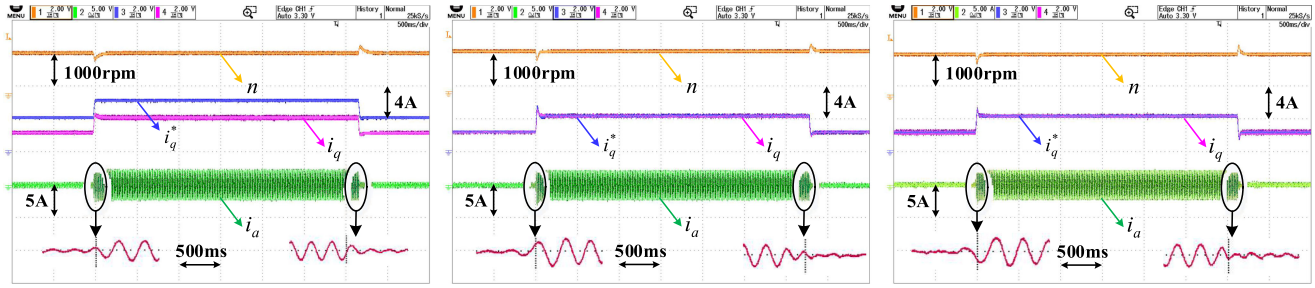

Fig. 10. Comparison of three controllers at step change of load torque (1 N·m) with parameter mismatch ($R_0 = 0.75R$, $L_0 = 0.75L$, and $\psi_{f0} = 0.75\psi_f$) under 1000 r/min. (a) Conventional DPCC. (b) ISMC-based DPCC ($M_d = 8$, $M_q = 10$, $\tau_d = 200$, $\tau_q = 150$, $\eta_d = 0.92$, and $\eta_d = 0.99$). (c) ISMC-based DPCC with STA chattering attenuation ($h_d = 150\,000$, $\eta_d = 0.5$, $h_q = 300\,000$, and $\eta_d = 0.64$).

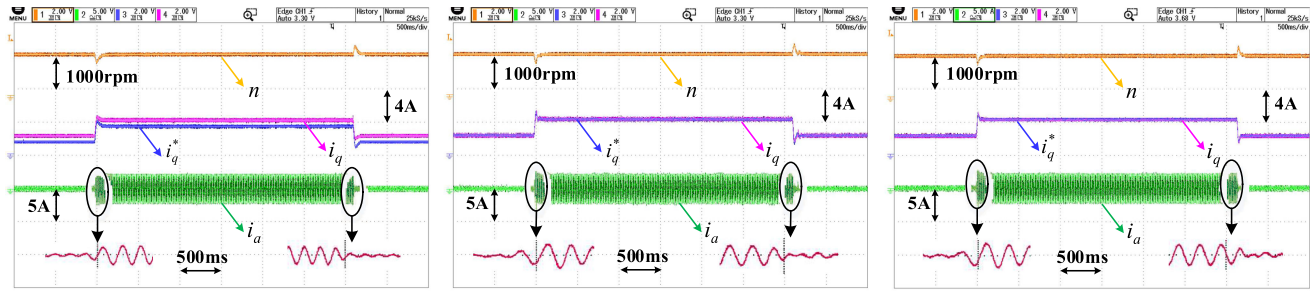

Fig. 11. Comparison of three controllers at step change of load torque (1 N·m) with parameter mismatch ($R_0 = 1.25R$, $L_0 = 1.25L$, and $\psi_{f0} = 1.25\psi_f$) under 1000 r/min. (a) Conventional DPCC. (b) ISMC-based DPCC ($M_d = 8$, $M_q = 10$, $\tau_d = 200$, $\tau_q = 120$, $\eta_d = 0.92$, and $\eta_d = 0.99$). (c) ISMC-based DPCC with STA chattering attenuation ($h_d = 150\,000$, $\eta_d = 0.5$, $h_q = 300\,000$, and $\eta_d = 0.64$).

mismatch, an external disturbance simulated by a step change of load torque (1 N·m) is exerted and released at 1 s and 4.2 s, respectively. In Fig. 10, the nominal values of the three parameters are set smaller than the real value ($R_0 = 0.75R$, $L_0 = 0.75L$, and $\psi_{f0} = 0.75\psi_f$), whereas in Fig. 11, the nominal values are larger than the actual ones ($R_0 = 1.25R$, $L_0 = 1.25L$, and $\psi_{f0} = 1.25\psi_f$). The tracking error of the q-axis current is about 2 A and the speed recovery time is about 0.18 s by the conventional PCC method in Fig. 10(a), whereas by the proposed ISMC-based PCC method, the tracking error is fully canceled in (b) and (c). Additionally, the speed recovery time decreases largely to about 0.06 s in (b) and (c). From Fig. 11, the current tracking error is about 0.5 A and the recovery time is about 0.15 s in (a) by the conventional DPCC method. Clearly in (b) and (c), the motor performance is significantly improved in terms of speed recovery time (0.08 s) and the current tracking ability (zero steady-state error). Compared with the ISMC with signum function, it can be observed that both the overshoot and the chattering are smaller with the improved STA method further applied.

In summary, according to the experimental results, it is proved that the proposed method has satisfying current control

performance. The disturbance rejection ability against parameter mismatch and sudden change of external load torque is also proved without damaging the system's overall performance.

VI. Conclusion

This article is an extension of the conventional DPCC method that grants disturbance rejection ability to the system against lumped disturbance by a novel ISMC method. Meanwhile, implementation steps and several issues in practical applications have been discussed. Even if the chattering effect introduced by the disturbance rejection term is significantly attenuated by an STA method, it is still unavoidable when large disturbance occurs. Future works will include the motor parameter identification since the more accurate the nominal values are, the smaller gains are needed to ensure convergence, which is a feasible method for further chattering attenuation.

References

[1] M. Zhou, X. Zhang, W. Zhao, J. Ji, and J. Hu, "Influence of magnet shape on the cogging torque of a surface-mounted permanent magnet motor," *Chin. J. Elect. Eng.*, vol. 5, no. 4, pp. 40–50, Dec. 2019.

[2] B.-J. Kang and C.-M. Liaw, "A robust hysteresis current-controlled PWM inverter for linear PMSM driven magnetic suspended positioning system," *IEEE Trans. Ind. Electron.*, vol. 48, no. 5, pp. 956–967, Oct. 2001.

[3] M. P. Kazmierkowski and L. Malesani, "Current control techniques for three-phase voltage-source PWM converters: A survey," *IEEE Trans. Ind. Electron.*, vol. 45, no. 5, pp. 691–703, Oct. 1998.

[4] Y. Jiang, W. Xu, C. Mu, and Y. Liu, "Improved deadbeat predictive current control combined sliding mode strategy for PMSM drive system," *IEEE Trans . Veh. Technol.*, vol. 67, no. 1, pp. 251–263, Jan. 2018.

[5] S. Kouro, P. Cortes, R. Vargas, U. Ammann, and J. Rodriguez, "Model predictive control—A simple and powerful method to control power converters," *IEEE Trans. Ind. Electron.*, vol. 56, no. 6, pp. 1826–1838, Jun. 2009.

[6] Z. Wang, A. Yu, X. Li, G. Zhang, and C. Xia, "A novel current predictive control based on fuzzy algorithm for PMSM," *IEEE Trans. Emerg. Sel. Topics Power Electron.*, vol. 7, no. 2, pp. 990–1001, Jun. 2019.

[7] M. S. Suryakant and M. Singh, "Performance analysis of PMSM drive using hysteresis current controller and PWM current controller," in *Proc. IEEE Students' Conf. Elect. Electron. Comput. Sci.*, Mar. 2018, pp. 1–5.

[8] J. Gao, S. Li, Y. Xu, and J. Zou, "Time-delay compensation method in PMSM servo system based on predictive current control with sensitivity analysis," in *Proc. 22nd Int. Conf. Electr. Mach. Syst.*, Aug. 2019, pp. 1–6.

[9] A. Wang, X. Jia, and S. Dong, "A new exponential reaching law of sliding mode control to improve performance of permanent magnet synchronous motor," *IEEE Trans. Magn.*, vol. 49, no. 5, pp. 2409–2412, May 2013.

[10] S. Vazquez, J. Rodriguez, M. Rivera, L. G. Franquelo, and M. Norambuena, "Model predictive control for power converters and drives: Advances and trends," *IEEE Trans. Ind. Electron.*, vol. 64, no. 2, pp. 935–947, Feb. 2017.

[11] P. Wipasuramonton, Z. Q. Zhu, and D. Howe, "Predictive current control with current-error correction for PM brushless AC drives," *IEEE Trans. Ind. Appl.*, vol. 42, no. 4, pp. 1071–1079, Jul./Aug. 2006.

[12] H. A. Young, M. A. Perez, and J. Rodriguez, "Analysis of finite-control-set model predictive current control with model parameter mismatch in a three-phase inverter," *IEEE Trans. Ind. Electron.*, vol. 63, no. 5, pp. 3100–3107, May 2016.

[13] R. J. Kerkman, D. Leggate, D. W. Schlegel, and C. Winterhalter, "Effects of parasitics on the control of voltage source inverters," *IEEE Trans. Power Electron.*, vol. 18, no. 1, pp. 140–150, Jan. 2003.

[14] P. Cortes, J. Rodriguez, C. Silva, and A. Flores, "Delay compensation in model predictive current control of a three-phase inverter," *IEEE Trans. Ind. Electron.*, vol. 59, no. 2, pp. 1323–1325, Feb. 2012.

[15] H. Le-Huy, K. Slimani, and P. Viarouge, "Analysis and implementation of a real-time predictive current controller for permanent-magnet synchronous servo drives," *IEEE Trans. Ind. Electron.*, vol. 41, no. 1, pp. 110–117, Feb. 1994.

[16] T. Türker, U. Buyukkeles, and A. F. Bakan, "A robust predictive current controller for PMSM drives," *IEEE Trans. Ind. Electron.*, vol. 63, no. 6, pp. 3906–3914, Jun. 2016.

[17] M. Siami, D. A. Khaburi, A. Abbaszadeh, and J. Rodríguez, "Robustness improvement of predictive current control using prediction error correction for permanent-magnet synchronous machines," *IEEE Trans. Ind. Electron.*, vol. 63, no. 6, pp. 3458–3466, Jun. 2016.

[18] J. Yang, W. Chen, S. Li, L. Guo, and Y. Yan, "Disturbance/uncertainty estimation and attenuation techniques in PMSM drives—A survey," *IEEE Trans. Ind. Electron.*, vol. 64, no. 4, pp. 3273–3285, Apr. 2017.

[19] W. Chen, J. Yang, L. Guo, and S. Li, "Disturbance-observer-based control and related methods—An overview," *IEEE Trans. Ind. Electron.*, vol. 63, no. 2, pp. 1083–1095, Feb. 2016.

[20] K.-H. Kim, I.-C. Baik, G.-W. Moon, and M.-J. Youn, "A current control for a permanent magnet synchronous motor with a simple disturbance estimation scheme," *IEEE Trans. Control Syst. Technol.*, vol. 7, no. 5, pp. 630–633, Sep. 1999.

[21] B. Wang, X. Chen, Y. Yu, G. Wang, and D. Xu, "Robust predictive current control with online disturbance estimation for induction machine drives," *IEEE Trans. Power Electron.*, vol. 32, no. 6, pp. 4663–4674, Jun. 2017.

[22] C. Xu, Z. Han, and S. Lu, "Deadbeat predictive current control for permanent magnet synchronous machines with closed-form error compensation," *IEEE Trans. Power Electron.*, vol. 35, no. 5, pp. 5018–5030, May 2020.

[23] Z. Q. Zhu, D. Liang, and K. Liu, "Online parameter estimation for permanent magnet synchronous machines: An overview," *IEEE Access*, vol. 9, pp. 59059–59084, 2021.

[24] Y. A. I. Mohamed and E. F. El-Saadany, "Robust high bandwidth discrete-time predictive current control with predictive internal model—A unified approach for voltage-source PWM converters," *IEEE Trans. Power Electron.*, vol. 23, no. 1, pp. 126–136, Jan. 2008.

[25] R. Yang, M. Wang, L. Li, C. Zhang, and J. Jiang, "Robust predictive current control with variable-gain adaptive disturbance observer for PMLSM," *IEEE Access*, vol. 6, pp. 13158–13169, 2018.

[26] Y. Yao, Y. Huang, F. Peng, J. Dong, and H. Zhang, "An improved deadbeat predictive current control with online parameter identification for surface-mounted PMSMs," *IEEE Trans. Ind. Electron.*, vol. 67, no. 12, pp. 10145–10155, Dec. 2020.

[27] M. Yang, X. Lang, J. Long, and D. Xu, "Flux immunity robust predictive current control with incremental model and extended state observer for PMSM drive," *IEEE Trans. Power Electron.*, vol. 32, no. 12, pp. 9267–9279, Dec. 2017.

[28] X. Zhang, B. Hou, and Y. Mei, "Deadbeat predictive current control of permanent-magnet synchronous motors with stator current and disturbance observer," *IEEE Trans. Power Electron.*, vol. 32, no. 5, pp. 3818–3834, May 2017.

[29] X. Zhang, L. Zhang, and Y. Zhang, "Model predictive current control for PMSM drives with parameter robustness improvement," *IEEE Trans. Power Electron.*, vol. 34, no. 2, pp. 1645–1657, Feb. 2019.

[30] X. Sun, J. Cao, G. Lei, Y. Guo, and J. Zhu, "A robust deadbeat predictive controller with delay compensation based on composite sliding-mode observer for PMSMs," *IEEE Trans. Power Electron.*, vol. 36, no. 9, pp. 10742–10752, Sep. 2021.

[31] R. Yang, M. Wang, L. Li, Y. Zenggu, and J. Jiang, "Integrated uncertainty/disturbance compensation with second-order sliding-mode observer for PMLSM-driven motion stage," *IEEE Trans. Power Electron.*, vol. 34, no. 3, pp. 2597–2607, Mar. 2019.

[32] Y. Zhang, J. Jin, and L. Huang, "Model-free predictive current control of PMSM drives based on extended state observer using ultralocal model," *IEEE Trans. Ind. Electron.*, vol. 68, no. 2, pp. 993–1003, Feb. 2021.

[33] D. Ke, F. Wang, L. He, and Z. Li, "Predictive current control for PMSM systems using extended sliding mode observer with Hurwitz-based power reaching law," *IEEE Trans. Power Electron.*, vol. 36, no. 6, pp. 7223–7232, Jun. 2021.

[34] Y. Shtessel, C. Edwards, L. Fridman, and A. Levant, *Sliding Mode Control and Observation*, 1st ed. New York, NY, USA: Birkhäuser, Nov. 2014.

[35] Y. Pan, C. Yang, L. Pan, and H. Yu, "Integral sliding mode control: Performance, modification, and improvement," *IEEE Trans. Ind. Informat.*, vol. 14, no. 7, pp. 3087–3096, Jul. 2018.

[36] F. Tinazzi, P. G. Carlet, S. Bolognani, and M. Zigliotto, "Motor parameter-free predictive current control of synchronous motors by recursive least-square self-commissioning model," *IEEE Trans. Ind. Electron.*, vol. 67, no. 11, pp. 9093–9100, Nov. 2020.

[37] J. Zhang, X. Liu, Y. Xia, Z. Zuo, and Y. Wang, "Disturbance observer-based integral sliding-mode control for systems with mismatched disturbances," *IEEE Trans. Ind. Electron.*, vol. 63, no. 11, pp. 7040–7048, Nov. 2016.

[38] B. Kürkçü, C. Kasnakoğlu, and M. Ö. Efe, "Disturbance/uncertainty estimator based integral sliding-mode control," *IEEE Trans Autom. Control*, vol. 63, no. 11, pp. 3940–3947, Nov. 2018.
[39] J. Wang, X. Luo, L. Wang, Z. Zuo, and X. Guan, "Integral sliding mode control using a disturbance observer for vehicle platoons," *IEEE Trans. Ind. Electron.*, vol. 67, no. 8, pp. 6639–6648, Aug. 2020.
[40] K. Ogata, *Discrete-time Control System,* 2nd ed. Minneapolis, MN, USA: Prentice-Hall, 2006.
[41] V. Utkin, J. Guldner, and J. Shi, *Sliding Mode Control in Electro-Mechanical Systems*, 2nd ed. Boca Raton, FL, USA: CRC Press, 2009.
[42] A. Chalanga, S. Kamal, L. M. Fridman, B. Bandyopadhyay, and J. A. Moreno, "Implementation of super-twisting control: Super-twisting and higher order sliding-mode observer-based approaches," *IEEE Trans. Ind. Electron.*, vol. 63, no. 6, pp. 3677–3685, Jun. 2016.
[43] J. A. Moreno and M. Osorio, "Strict Lyapunov functions for the super-twisting algorithm," *IEEE Trans Autom. Control*, vol. 57, no. 4, pp. 1035–1040, Apr. 2012.
[44] J. Rodriguez and P. Cortes, *Predictive Control of Power Converters and Electrical Drives*, 1st ed. Valparaiso, Chile: Wiley, 2012.

Yongxiang Xu (Member, IEEE) received the M.S. and Ph.D. degrees in electrical engineering from the Harbin Institute of Technology, Harbin, China, in 2001 and 2005, respectively.

In 2005, he joined the Department of Electrical Engineering, Harbin Institute of Technology, as an Assistant Professor. Since 2013, he has been a Professor with the Department of Electrical Engineering, Harbin Institute of Technology. His current research interests include permanent-magnet machine design and control.

Shaobin Li was born in Liaoning Province, China, in 1997. He received the B.S. degree in electrical engineering in 2019 from the Harbin Institute of Technology, Harbin, China, where he is currently working toward the Ph.D. degree with the School of Electrical Engineering and Automation.

His current research interests include permanent-magnet motor drives and control.

Jibin Zou (Senior Member, IEEE) received the M.S. and Ph.D. degrees in electrical engineering from the Harbin Institute of Technology, Harbin, China, in 1984 and 1988, respectively.

Since 1985, he has been engaged in the research of electrical machines. He was a Visiting Research Fellow with the University of Liverpool, Liverpool, U.K., for one year. He is currently a Professor with the State Key Laboratory of Robotics and System, Harbin Institute of Technology. His current research interests include permanent-magnet machine design and control.

Prof. Zou has been a Senior Member of the IEEE Magnetics Society since 2000.